APPLICATION OF FATIGUE FRACTURE MECHANICS TO CIVIL ENGINEERING STRUCTURES

Andrea Carpinteri and Roberto Brighenti

University of Parma
Department of Civil Engineering
Viale delle Scienze, 43100 Parma, Italy

Abstract. Fatigue fracture mechanics concepts can usefully be applied in the field of civil engineering for both metallic and reinforced concrete structures. Two examples are shown in this paper. Firstly, the fatigue growth of surface cracks in metallic round bars is examined by numerically obtaining the propagation patterns for different material properties and loading conditions. Secondly, the behaviour of a reinforced concrete beam cross-section subjected to a cyclic bending moment is analyzed by a fracture mechanics model and, in particular, the energy dissipated during the loading and unloading processes is calculated from the hysteretic loops in the moment-rotation diagram. Experimental tests validate the theoretical results obtained for the two above problems.

Abstract (Italian). Concetti di "meccanica della frattura e fatica" possono essere utilmente applicati nel campo dell'ingegneria civile per strutture metalliche o in calcestruzzo armato. Due esempi vengono illustrati in questa nota. Dapprima viene esaminata la crescita a fatica di fessure superficiali in barre metalliche di sezione circolare, ottenendo per via numerica i percorsi di propagazione per diversi materiali e condizioni di carico. Successivamente viene analizzato il comportamento della sezione trasversale di una trave in calcestruzzo armato soggetta a momento flettente ciclico mediante un modello basato sulla meccanica della frattura e, in particolare, l'energia dissipata durante i processi di carico e scarico viene calcolata dai cicli di isteresi nel diagramma momento-rotazione. Prove sperimentali convalidano i risultati teorici ottenuti per i due problemi esaminati.

1. INTRODUCTION

As is well-known, several failures of civil engineering structures occur due to cyclic loading. As a matter of fact, a cyclically time-varying loading reduces the material strength and can provoke a fatigue failure which consists of three stages: (a) crack initiation (from microcrack initiation to engineering-size flaw formation), (b) crack propagation, and (c) catastrophic failure. The conventional (or classical) fatigue design approach, which involves the use of the "stress - fatigue life" (S-N) curves developed from endurance tests, does not distinguish between crack initiation and crack propagation, while the approach currently used is the *fatigue fracture mechanics* approach, the aim of which is to understand the fatigue crack initiation and propagation phenomena since it is often very important to predict the fatigue life of a structural component after a crack has initiated [1].

Two applications of fatigue fracture mechanics concepts to civil engineering structures are shown in the following. Firstly, the crack growth patterns for elliptical-arc surface flaws in ciclically loaded metallic round bars are obtained by a numerical investigation based on Paris-Ergodan law [2]. The replacement of an actual part-through defect by an equivalent elliptical-arc flaw is reasonable since many experimental analyses support this assumption. Different initial crack sizes, material properties and loading conditions are considered and, for each case examined, it is deduced that these flaws tend to follow preferred propagation paths which converge to an inclined asymptote in the diagram of flaw aspect ratio against relative crack depth of the deepest point on the crack front.

Secondly, a reinforced concrete beam cross-section under cyclic bending moment is analyzed. A shake-down phenomenon due to steel plastic flow occurs when the maximum bending moment is greater than or equal to the value of slippage or yielding of the reinforcement and lower than the value of unstable fracture of concrete. When a crack develops, the hysteretic loops described in the moment-rotation diagram shift toward the right-hand side and a numerical procedure can follow the fatigue crack growth and calculate the energy dissipated during the phenomenon.

2. FATIGUE CRACK PROPAGATION IN METALLIC ROUND BARS

2.1 Stress-Intensity Factors for Surface Cracks

Many authors have analyzed the stress-intensity factor variation along the front of surface flaws in metallic round bars [3-20], and the reader can find additional references on the subject in Ref.[1]. The results of these analyses are very useful for reliable predictions of fatigue crack propagation.

Consider an elliptical-arc edge flaw under tension or bending loading (Fig.1). The flaw aspect ratio $r = a / b$ and the relative depth $\xi = a / D$ of the deepest point A on the defect front define the crack configuration being examined. The generic point P along the front is identified by the normalized coordinate ζ / h. The axial force F acts perpendicularly to the crack plane, while the bending moment M acts about an axis parallel to the semi-major axis b of the elliptical front.

The parameter ξ is made to vary from 0.1 to 0.6, whereas the aspect ratio r ranges from 0.0 (straight front) to 1.0 (circular-arc front). For each couple of values assumed for the above geometrical parameters, the stress field has been obtained through a three-dimensional finite element analysis carried out by using 20-node isoparametric solid elements [16,17]. The stress square-root singularity was modelled by shifting the finite element midside nodes near the crack front to quarter-point positions.

As is known, the singularity power at the flaw border point B depends on the material Poisson ratio ν and on the intersection angle β between crack front and external surface, and is generally different from 0.5 even if it does not remarkably deviate from this value. Therefore, the use of quarter-point finite elements (square-root singularity) does not produce reliable results in a boundary layer near point B, but this effect is confined only in a small zone.

The dimensionless stress-intensity factors for both tension and bending are obtained as follows :

$$\tilde{K}_{I,F} = \frac{K_{I,F}}{\sigma_F \, (\pi \, a)^{1/2}} \qquad (1)$$

$$\tilde{K}_{I,M} = \frac{K_{I,M}}{\sigma_M \, (\pi \, a)^{1/2}} \qquad (2)$$

where

$\sigma_F = F / (\pi \, D^2 / 4)$ = applied uniform tensile stress,

$\sigma_M = M / (\pi \, D^3 / 32)$ = maximum bending stress.

As discussed in Refs [1,17], for each value of the crack depth ξ the maximum stress-intensity factor is attained near the external surface in the case of r = 1.0 (circular-arc flaw) and at point A in the case of r = 0.0 (straight-fronted flaw) (Fig.2). Therefore it is possible to qualitatively predict that, for both tension and bending, a circular-arc crack tends to flatten, while a straight crack tends to become curved, as deduced by other authors [5,8,9].

For intermediate values of flaw aspect ratio ($0.0 < r < 1.0$), a transition phenomenon is noticed, that is, the stress-intensity factor reaches the maximum at point A for $r \le r_t$ and near point B for $r \ge r_t$, with r_t = transition aspect ratio. For example, Figure 2 shows that, when $\xi = 0.3$, the above transition occurs for $r_t = 0.70$ in the case of tension and for $r_t = 0.55$ in the case of bending.

2.2 Fatigue Crack Propagation

Several authors have analytically and experimentally deduced that the front of a surface flaw in a metallic round bar can be modelled quite accurately by an elliptical arc during the whole fatigue growth [1,5,6,8, 9,19,20]. On the other hand, the aspect ratio r changes under cyclic loading, and this significantly affects the fatigue life prediction for round bars. The above problem can be examined by a two-parameter model based on the Paris-Erdogan law [2] :

$$da / dN = A \, (\Delta K_I)^m , \qquad (3)$$

where

da / dN = crack propagation rate,

ΔK_I = stress-intensity factor range,

A and m = constants of the material.

If the ellipse centre is assumed to lie on the bar circumference (Fig.3), the crack front with semi-axes a and b will grow after one cyclic loading step to the new configuration [19] :

$$\frac{x^2}{(b^*)^2} + \frac{y^2}{(a^*)^2} = 1 \qquad (4)$$

where the two unknowns a* and b* can be obtained by the condition that the coordinates of the points A* and C* , deduced from Eqn (3), must satisfy Eqn (4).

As an example, Figure 4 shows the propagation patterns (thick lines) numerically obtained for cyclic tension loading with constant stress range $\Delta\sigma_F = 100$ Nmm^{-2}. The initial flaws examined have relative crack depth $\xi = a / D$ equal to 0.05, 0.10 or 0.20, and crack aspect ratio $r = a / b$ equal to 0.001 (straight front), 0.25, 0.50 or 1.00 (circular front). For each initial crack configuration analyzed, the propagation path tends to converge to an inclined asymptote in the diagram of r against ξ :

$$r = - 1.144 \, \xi + 1.365 \qquad (5)$$

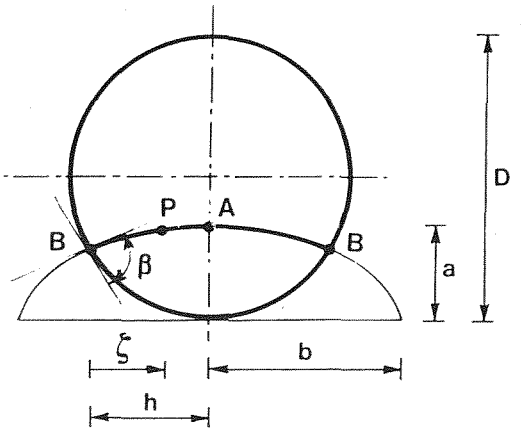

Fig. 1. Elliptical-arc flaw in a metallic round bar : geometrical parameters.

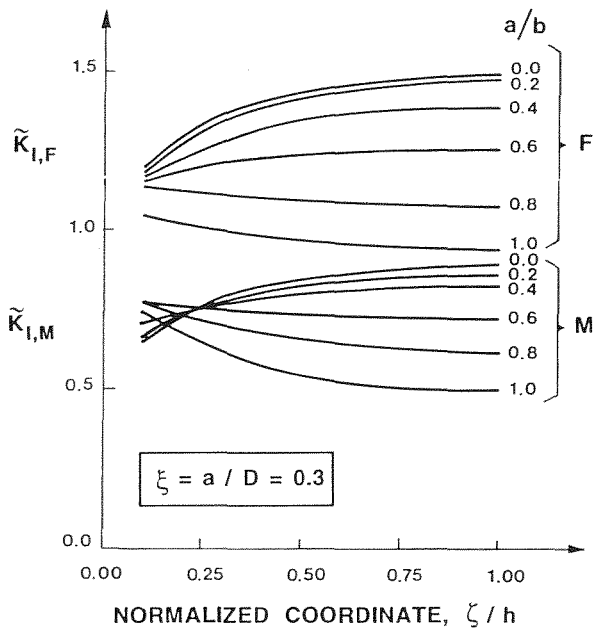

Fig. 2. Dimensionless stress-intensity factors for both tension and bending loading [1,17].

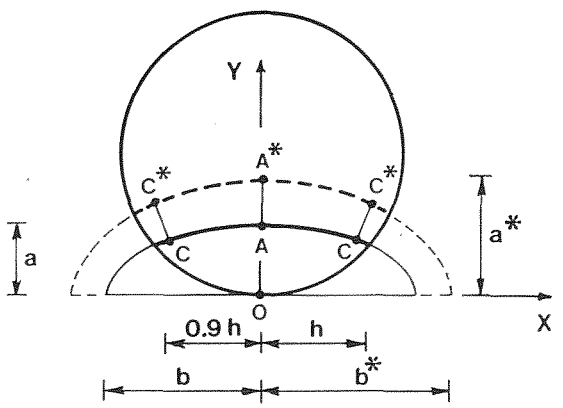

Fig. 3. Crack propagation after one cyclic loading step [19].

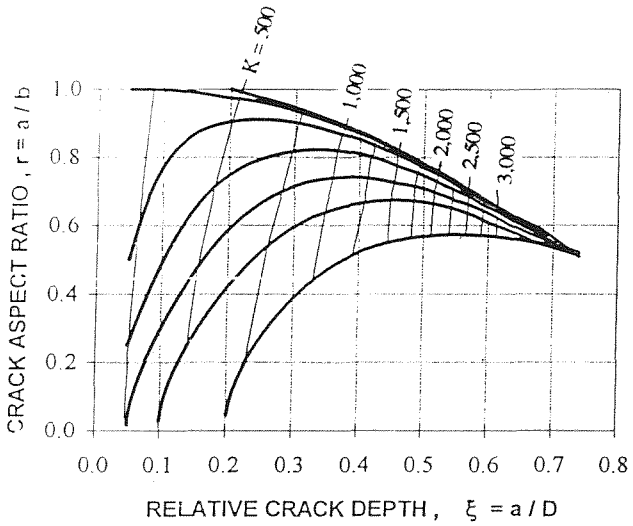

Fig. 4. Fatigue propagation paths (thick lines) for different initial crack configurations under tension, with $\Delta\sigma_F$ = 100 N mm^{-2}, m = 2 and A = 1.64 x 10^{-10}. Some iso-K curves (thin lines) are also displayed, with K ranging from 250 to 3,000 N mm$^{-3/2}$.

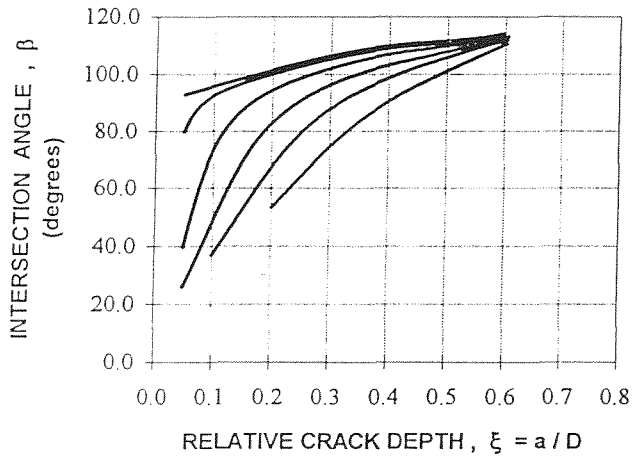

Fig. 5. Intersection angle β against relative crack depth ξ for the propagation paths plotted in Fig.4 (cyclic tension).

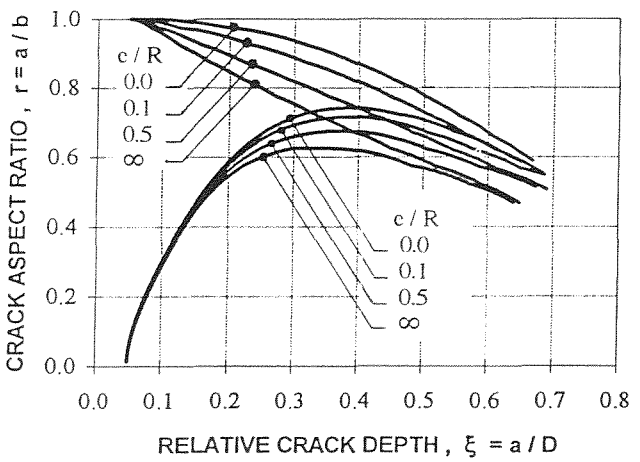

Fig. 6. Fatigue propagation paths under combined tension and bending, with $\Delta\sigma_t$ = 100 N mm^{-2}, m = 2 and A = 1.64 x 10^{-10}. The relative loading eccentricity e/R (with e = M / F and R = D / 2) is equal to 0, 0.1, 0.5 and ∞, respectively.

In particular, r is equal to about 0.6 ~ 0.7 for $\xi = 0.6$. It has been verified that several experimental data reported in the literature lie on the theoretical curves of Fig.4.

Note that some iso-K curves (thin lines) are also displayed in Fig.4, that is, the crack configurations where the maximum stress-intensity factor attains a given value are connected in the above diagram. More precisely, the maximum stress-intensity factor value ranges from 250 to 3,000 N mm$^{-3/2}$, with the curves plotted every 250 N mm$^{-3/2}$. It can be remarked that the iso-K curves become about vertical for $K_I \geq 1{,}500$ N mm$^{-3/2}$. In other words, when K_I is greater than the above value, the stress-intensity factor is almost independent of the parameter r, and that occurs for $\xi > 0.4 \sim 0.5$. Moreover, for $\xi > 0.5 \sim 0.6$ the K_I values are greater than the fatigue fracture toughness K_{fC} of the metallic materials usually employed in the civil engineering field, which means that the theoretical propagation paths in Fig.4 are real only for relative crack depth smaller than the above values.

The intersection angle β (Fig.1) against the parameter ξ is shown in Fig.5 for the seven cases examined in Fig.4 (note that two curves in Fig.5 are superimposed). From fracture energy considerations, some authors have theoretically deduced that the crack growth process requires a square-root singularity and, consequently, β has to be equal to about 100° for $\nu = 0.3$ and Mode I [1]. As can be observed in Fig.5, the intersection angle numerically obtained tends to values very close to the above theoretical result.

The same conclusions on the fatigue crack growth in round bars can be drawn for different initial crack sizes, material properties and loading conditions. For example, the propagation paths for combined tension and bending with stress range $\Delta\sigma_t = 100$ N mm^{-2} are presented in Fig.6 for two initial crack configurations and different values of the relative loading eccentricity e / R, where

$$\Delta\sigma_t = \Delta\sigma_F + \Delta\sigma_M = \Delta\sigma_F \, [1 + 4\,(e/R)] \qquad (6)$$

with $e = M/F$ and $R = D/2$. Note that $e/R = 0$ corresponds to pure extension and $e/R = \infty$ to pure bending. It can be remarked that the propagation paths do not change appreciably for e / R greater than about 1 (one), that is, bending effect dominates in this range.

3. CYCLICALLY LOADED REINFORCED CONCRETE BEAM CROSS-SECTION

3.1 Hysteretic Fracture Mechanics Model

Several authors have analyzed the behaviour of reinforced concrete structural elements, pointing out the hysteretic phenomena which can occur under cyclic loading [21-24].

The fracture mechanics model proposed in Ref's [25-28] examines the response of a rectangular reinforced concrete beam cross-section subjected to a cyclic bending moment M (Fig.7). If a through-thickness edge crack is assumed to develop in the stretched part, the bending moment M tends to open the crack whereas the eccentric axial force F due to the steel reinforcement reaction tends to close it.

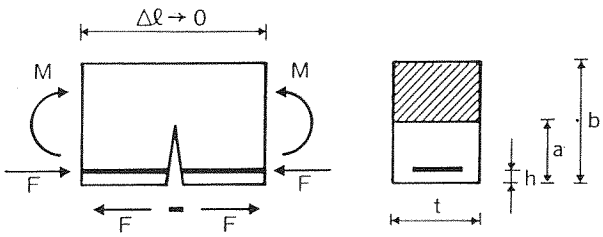

Fig. 7. Reinforced concrete beam cross-section under cyclic bending moment.

The rotation of the cross-section is assumed to be equal to zero up to the moment when steel yields :

$$\phi = \lambda_{MM} \, [M - F\,(b/2 - h)] + \lambda_{MF} \, [-F] = 0 \qquad (7)$$

where λ_{MM} and λ_{MF} are the local compliances for bending and extension/bending interaction, respectively. These compliances depend on ξ and the mechanical and geometrical properties of the cross-section [1,25-28]. Applying this congruence condition, the bending moment M_P of steel plastic flow can be computed :

$$M_P = F_P \, b \, [0.5 - (h/b) + r(\xi)] \qquad (8)$$

where F_P represents the force of yielding $f_y \, A_s$, with f_y = steel yield strength and A_s = steel area, and $r(\xi)$ is a function of ξ, with $\xi = a/b$. When the force of yielding is higher than the force of pulling-out, F_P indicates the latter, and a slippage phenomenon occurs.

If the maximum cyclic bending moment M is greater than M_P (point A in Fig.8), a residual rotation remains when the cross-section is unloaded (point B), and therefore the concrete compresses the steel reinforcement. By assuming a rigid - perfectly plastic behaviour of the steel, the congruence condition for obtaining the unknown steel compression is that the residual rotation is equal to the under-loading rotation :

$$\lambda_{MM} \, [F\,(b/2 - h)] + \lambda_{MF} \, [F] = \lambda_{MM} \, [M - F_P\,(b/2 - h)] + \lambda_{MF} \, [-F_P] \qquad (9)$$

Therefore the bending moment M_{SD} of plastic shakedown for which the steel compression is equal to F_P can be determined from Eqn (9) :

$$M_{SD} = 2\,F_P \, b \, [0.5 - (h/b) + r(\xi)] \qquad (10)$$

By comparing Eqn (8) with Eqn (10), it can be deduced that $M_{SD} = 2\,M_P$.

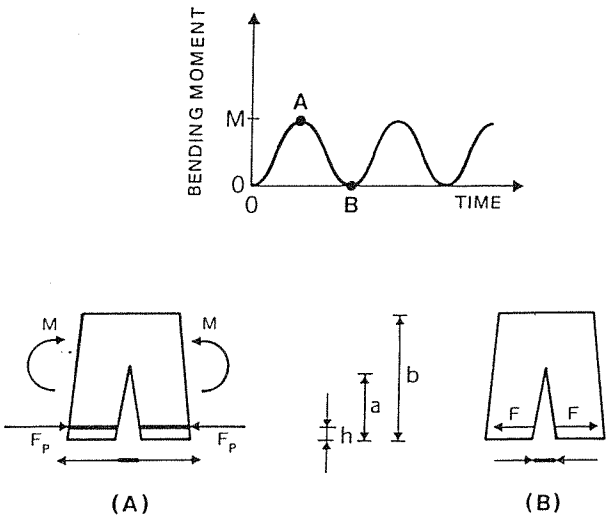

Fig. 8. Reinforced concrete beam cross-section: (A) under maximum loading; (B) after unloading.

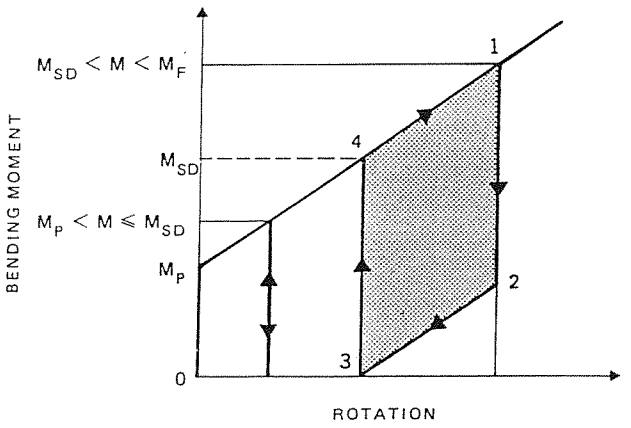

Fig. 9. Bending moment against rotation for the steel reinforcement [25-28].

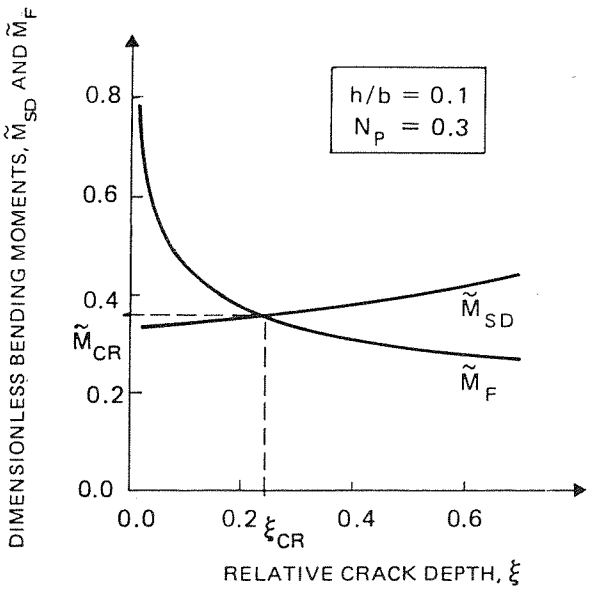

Fig. 10. Dimensionless bending moments against relative crack depth (for h/b = 0.1 and Np = 0.3) [27-28].

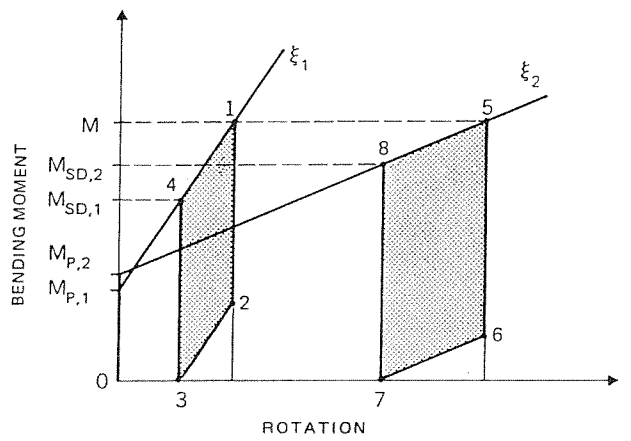

Fig. 11. Fatigue crack growth from ξ_1 to ξ_2 and related hysteretic loops in the moment rotation diagram [27-28].

In conclusion, if the beam cross-section is subjected to a cyclic bending moment with maximum value M, the following situations can occur (Fig.9) :

(1) elastic behaviour for $0 \le M < M_P$;
(2) elastic shake-down for $M_P \le M < M_{SD}$;
(3) plastic shake-down for $M_{SD} \le M < M_F$, where M_F is the unstable concrete fracture bending moment calculated by equalling the stress-intensity factor to the concrete fracture toughness.

In case No.3 the energy dissipated in each hysteretic loop (area 1-2-3-4 in Fig.9) can easily be calculated [25-28]. Note that the cyclic loading has been assumed to be unidirectional (see Figs 8 and 9), but analogous conclusions could be drawn for reversed cyclic loading.

3.2 Fatigue Crack Growth

The bending moments M_{SD} and M_F can be written in dimensionless form as functions of the parameters h / b, ξ and N_P , with N_P dependent on the mechanical and geometrical properties of the reinforced concrete beam cross-section [27,28].

The above dimensionless bending moments against the relative crack depth are plotted in Fig.10 for h / b = 0.1 and $N_P = 0.3$, and qualitatively analogous diagrams can be obtained for different values of these two parameters. In particular, the dimensionless $\tilde{M}_{SD}$ increases by increasing ξ, while the other curve decreases. The two curves intersect at a critical point, the coordinates of which are ξ_{CR} and $\tilde{M}_{CR}$ (Fig.10). Therefore, the plastic shake-down phenomenon cannot occur for $\xi \ge \xi_{CR}$ because it is preceded by the unstable concrete fracture ($\tilde{M}_F \le \tilde{M}_{SD}$).

Since it has been shown that ξ_{CR} decreases by increasing N_P [27,28], the plastic shake-down can occur only for low values of ξ if N_P is large. Note that the parameter N_P is large for high values of the size b, the steel percentage and the steel yield strength and/or for low values of concrete fracture toughness.

If the generic crack depth is equal to ξ_1 , the hardening line slope is λ_{MM}^{-1} calculated for $\xi = \xi_1$ (Fig.11), and the energy dissipated in each cycle is represented by the area 1-2-3-4. When the relative crack depth increases up to ξ_2 , the hardening line becomes more inclined, and the energy dissipated per cycle is equal to the area 5-6-7-8 (Fig.11). If ξ increases again, the hardening line is more and more inclined and the energy dissipated in the steel reinforcement can be calculated at each step.

In the case of dimensionless maximum bending moment $\tilde{M}$ greater than or equal to $\tilde{M}_{CR}$ (Fig.10) [27,28], the fatigue crack growth occurs from the initial relative crack depth (ξ_I) to the unstable fracture value (ξ_F), and the whole shake-down phenomenon is plastic. On the other hand, for $\tilde{M} < \tilde{M}_{CR}$ the crack growth occurs from ξ_I to ξ_F, but the shake-down is plastic only up to ξ_{SD} (relative depth for which $\tilde{M} = \tilde{M}_{SD}$).

The R.C. cross section behaviour predicted by the above fatigue fracture mechanics model was experimentally confirmed [26,28].

4. CONCLUSION

Fatigue fracture mechanics concepts have usefully been applied to civil engineering problems. Experimental tests validate the theoretical results obtained for both metallic and reinforced concrete structures subjected to cyclic loading.

5. REFERENCES

[1] A. Carpinteri (Editor), "Handbook of Fatigue Crack Propagation in Metallic Structures", Elsevier Science Publishers B.V., Amsterdam, The Netherlands (1994).

[2] P.C. Paris and F. Erdogan, "A critical analysis of crack propagation laws", Trans. American Soc. Mechanical Engineers (ASME), J. Basic Engng **85D**, 528-534 (1963).

[3] W.S. Blackburn, "Calculation of stress intensity factors for straight cracks in grooved and ungrooved shafts", Engng Fract. Mech. **8**, 731-736 (1976).

[4] M.A. Astiz and M. Elices, "On the application of the stiffness derivative method to two and three-dimensional fracture problems",Proc. 2nd Int. Conf. Numer. Meth. Fract. Mech., pp. 93-106 (1980).

[5] A. Athanassiadis, J.M. Boissenot, P. Brevet, D. François and A. Raharinaivo,"Linear elastic fracture mechanics computations of cracked cylindrical tensioned bodies", Int.J.Fract. **17**,553-566 (1981).

[6] W.D. Dover, "Crack shape evolution studies in threaded connections using A.C.F.M.", Fatigue Fract. Engng Mater. Struct. **5**, 349-353 (1982).

[7] H. Nisitani and D.H. Chen, "Stress intensity factor for a semi-elliptical surface crack in a shaft under tension", Trans. Japanese Society Mechanical Engineers (1984); in Stress Intensity Factors Handbook (Edited by Y. Murakami et al.), Vol. 2, pp.654-656, Pergamon Press, Oxford, U.K. (1987).

[8] R.G. Forman and V. Shivakumar,"Growth behavior of surface cracks in the circumferential plane of solid and hollow cylinders", In Fracture Mechanics:Seventeenth Volume, ASTM STP 905, pp. 59-74 (1986).

[9] M. Caspers, C. Mattheck and D. Munz, "Fatigue crack propagation in cylindrical bars", Z. Werkstofftech. **17**, 327-333 (1986).

[10] M.A. Astiz, "An incompatible singular elastic element for two- and three-dimensional crack problems", Int.J.Fract. **31**, 105-124 (1986).

[11] I.S. Raju and J.C. Newman,"Stress intensity factors for circumferential surface cracks in pipes and rods",

In Fracture Mechanics : Seventeenth Volume, ASTM STP 905, pp. 789-805 (1986).

[12]J. Llorca and V. Sánchez-Gálvez, "Fatigue threshold determination in high strength cold drawn eutectoid steel wires", Fatigue Fract. Engng Mater. Struct. **26**, 869-882 (1987).

[13]J. Llorca, J.M. Varona, V. Sánchez-Gálvez and F. Gutiérrez-Solana,"Fatigue behaviour of wire ropes", Mater.Struct. **22**, 411-419 (1989).

[14]J. Toribio, V. Sánchez-Gálvez, M.A. Astiz and J.M. Campos, "Stress intensity factor solutions for a cracked bolt under tension, bending and residual stress loading", Engng Fract. Mech. **39**, 359-371 (1991).

[15]J. Toribio, J.M. Campos and V. Sánchez-Gálvez, "X-ray measurement of residual stresses in a rolled bolt : application to the calculation of stress intensity factors after cracking", J. Strain Anal. **26**, 103-109 (1991).

[16]A. Carpinteri, "Stress-intensity factors for straight-fronted edge cracks in round bars", Engng Fract. Mech. **42**, 1035-1040 (1992).

[17]A. Carpinteri, "Elliptical-arc surface cracks in round bars", Fatigue Fract. Engng Mater. Struct. **15**, 1141-1153 (1992).

[18]J. Toribio, "Stress intensity factor solutions for a cracked bolt loaded by a nut", Int.J.Fract. **53**, 367-385 (1992).

[19]A. Carpinteri, "Shape change of surface cracks in round bars under cyclic axial loading", Int. J. Fatigue **15**, 21-26 (1993).

[20]A. Levan and J. Royer, "Part-circular surface cracks in round bars under tension, bending and twisting", Int.J.Fract. **61**, 71-99 (1993).

[21]S.P. Shah, "Prediction of cumulative damage for concrete and reinforced concrete", Mater. Struct. **17**, 65-68 (1984).

[22]F.C. Filippou, E.P. Popov and V.V. Bertero, "Analytical studies of hysteretic behavior of R/C joints", J. Struct.Division (ASCE) **112**, 1605-1622 (1986).

[23]M.L. Wang and S.P. Shah, "Reinforced concrete hysteresis model based on the damage concept", Earthquake Engng Struct. Dynam. **15**, 993-1003 (1987).

[24]S.P. Shah, M.L. Wang and L. Chung, "Model concrete beam-column joints subjected to cyclic loading at two rates", Mater. Struct. **20**, 85-95 (1987).

[25]Al. Carpinteri and An. Carpinteri, "Hysteretic behavior of R.C. beams", J. Struct. Engng (ASCE) **110**, 2073-2084 (1984).

[26]A. Carpinteri and F. Zaupa, "Behavior of R.C. beam cross sections under unidirectional cyclic bending moments", Proceedings of the 8th Biennial European Conference on Fracture, pp. 828-833, Turin , Italy (1990).

[27]A. Carpinteri, "Energy dissipation in R.C. beams under cyclic loadings", Engng Fract. Mech. **39**, 177-184 (1991).

[28]A. Carpinteri, "Reinforced concrete beam behavior under cyclic loadings", In Applications of Fracture Mechanics to Reinforced Concrete (Editor Al. Carpinteri), pp. 547-578, Elsevier Science Publishers, U.K. (1992).